

Physical Modelling of the SET/RESET characteristics and analog properties of $\text{TiO}_x/\text{HfO}_{2-x}/\text{TiO}_x$ -based RRAM devices

P. Bousoulas, P. Asenov, D. Tsoukalas
Department of Applied Physics
National Technical University of Athens
Heron Polytechniou 9, 15780 Athens, Greece
panbous@mail.ntua.gr

Abstract—Understanding the origins of switching effect is of great importance, since it can enlighten our perspectives and offers guidance for novel device design. In contrast with the common electronic devices which rely their operation only at electron transport properties, resistive switching effect exhibits a strong dependence from the local distribution of ions. Here, we present a quantitative analysis, both at DC and AC domains, which can account for the analog properties of our trilayer-based devices. Our approach can capture the gradual SET/RESET responses, which stem from the balance between drift and diffusion effect, and highlight the crucial role of temperature, electric field and oxygen vacancy density on the switching pattern.

I. INTRODUCTION

Resistive random access memory (RRAM) devices have opened a vast number of applications, ranging from non-volatile memories to logic circuits and neuromorphic systems [1-3]. Although, in many aspects their progress has surpassed their understanding, conducting filament (CF) theory seems to gain universal acceptance, based on concrete experimental [4] and theoretical proofs [5]. The main advantage of RRAM structures is that their conductivity is not exclusively dependent from the electron transport, but also is a strong function of the local oxygen vacancy (V_o) concentration. Thus, by employing defect engineering concepts, opportunities arise in order to confine the CF formation/annihilation into specific regions, reducing therefore the inherit degree of variability and the power consumption values of the memory cell as well as influence the switching pattern. In light of the above, bilayer [6] and trilayer [7] based structures, appears as a promising architecture since the switching phenomenon will take place on one of various layers, while the other layers will serve the role of a defect reservoir, sustaining thus the switching effect under electrical stressing operating conditions. On the other hand, these layers due to their highly defective nature will add a series resistance on the device electrical performance, diminishing hence current overshooting issues and decreasing the operation power. So, it is urgent to provide comprehensive models of the switching effect, which will account for the role of temperature, electric field and V_o density gradients.

In this work we present a physical model of $\text{TiO}_x/\text{HfO}_{2-x}/\text{TiO}_x$ trilayer memristor [8], which can interpret the gradual switching pattern at low operating current (\sim nA), both at DC and pulse operation conditions. Based on CF perception, regions with high density of V_o (TiO_x) can switch the device from a high resistance state (HRS) to a low resistance state (LRS), while the presence of the HfO_{2-x} layer can tune the diffusion barrier for oxygen vacancy migration, thus directly influencing the drift and diffusion fluxes.

II. EXPERIMENTAL

The RRAM devices were fabricated on Si/SiO_2 substrates. Initially, 40 nm Au was deposited by e-gun evaporation. Then TiO_x film growth took place by RF magnetron sputtering, from Ti target with 10/1.5 gas mixture of Ar/O_2 . Consequently, HfO_{2-x} was deposited by the same method, but from HfO_{2-x} target and with higher oxygen ratio (10/5) and then TiO_x was again deposited. All depositions were performed at room temperature, and each metal oxide layer has 25 nm thickness. Finally, Ti (4 nm) and TiN (40 nm) were used as top electrodes (TE), and patterned to form Metal-Insulator-Metal (MIM) capacitors, using lift-off lithography. The size of each square TE was $100 \times 100 \mu\text{m}^2$. Electrical characterization was performed with Keithley 4200 SCS.

III. RESULTS AND DISCUSSION

The simulation starts after the CF has already been formed, whereas the simulated geometry is presented at Fig. 2(a). The driving force for the resistance switching is the field and temperature induced migration of oxygen ions and the subsequent redistribution of V_o . Therefore, the total memristive behavior can be predicted by the ion transport, carrier continuity and Joule heating partial differential equations, which were solved self-consistently with a numerical solver (COMSOL) [9,10]:

$$\frac{\partial n_D}{\partial t} = \nabla \cdot (D \nabla n_D - v \cdot n_D) + G + R \quad (1)$$

$$\nabla \cdot \sigma \nabla \psi = 0 \quad (2)$$

$$-\nabla \cdot k_{th} \nabla T = J \cdot E \quad (3)$$

where n_D is the concentration of oxygen vacancies, $D = \frac{1}{2} \cdot a^2 \cdot v_0 \cdot \exp(-\frac{E_a}{k_B T})$ is the diffusivity, a is the

effective hopping distance (0.1 nm), v_0 is the attempt-to-escape frequency (10^{13} Hz), k_B is the Boltzmann constant, T is the temperature, ψ is the electric potential, E_a is the diffusion barrier for ion migration $E_a = E_a^{migration}$ (1 eV for HfO_{2-x}

and 1.5 eV for TiO_x), $v = a \cdot v_0 \cdot \exp(-\frac{E_a}{k_B T}) \cdot \sinh(\frac{QEa}{2k_B T})$

is the drift velocity of oxygen vacancies, E is the electric field and Q is the ionic charge (2q), $G = n_G \exp(-\frac{E_b - qaE}{k_B T})$ is the generation rate of V_o (used only at SET process - $E_b = 1$ eV) and $R = n_G \exp(-\frac{E_r}{k_B T})$ is the recombination of oxygen ions with V_o (used only for RESET process - $E_r = 1$ eV). In order to solve the set of equations self-consistently, inputs for electrical conductivity (σ) and thermal conductivity (k_{th}) are needed. Since CF is presumed to consist of oxygen vacancies, which act as local donors, it is reasonable to assume that the electrical conductivity will depend from the density of defects, by a thermally activated Arrhenius equation

$\sigma = \sigma_0 \exp(-\frac{E_{AC}}{k_B T})$ where σ_0 is a pre-exponential factor

and E_{AC} is the activation energy. As it is depicted in Fig. 1(b), σ_0 linearly increases from 0.5 to 800 Scm^{-1} with an increase of n_D , which corresponds to a value for electrical resistivity of 1 $m\Omega cm$ for the highest n_D . In addition, Fig. 1(c) shows the values for conduction activation energy, as these were extracted from Fig. 1(a), used in the simulations. The activation energy is 0.02 eV for high n_D and linearly increases to 0.07 eV with a decrease in n_D , indicating the semiconducting nature of a broken CF [11]. Furthermore, a linear dependence of k_{th} from the n_D was chosen, following the Wiedemann-Franz law. Thus for the minimum value of defect density ($n_D = 0$), a value of $k_{th} = 3 Wm^{-1}K^{-1}$ was selected, which approximately corresponds to the thermal conductivity of both TiO_{2-x} and HfO_{2-x} insulating states for $T = 300$ K. Consequently, for the maximum value of n_D , a thermal conductivity which corresponds to that of metallic CF, i.e. thermal conductivity of both titanium and hafnium $k_{th} = 22.5 Wm^{-1}K^{-1}$, was introduced. Although the linear approximations of σ_0 , E_{AC} and k_{th} from n_D appear to have weak physical background, the calculated results display good consistency with the experimental data.

The axisymmetric reduces one dimension from the problem, and the calculations are performed in 2D equivalent plane with radial coordinate r and vertical coordinate z . Both active oxide and electrodes are considered during the simulations ($\sigma_{Au} = 4.5 \times 10^7 Scm^{-1}$, $k_{Au} = 318 Wm^{-1}K^{-1}$,

$\sigma_{Ti} = 2.4 \times 10^6 Scm^{-1}$, $k_{Ti} = 21.9 Wm^{-1}K^{-1}$, $\sigma_{TiN} = 1 \times 10^6 Scm^{-1}$, $k_{TiN} = 28.8 Wm^{-1}K^{-1}$).

The corresponding boundary conditions used are the following: $\psi = 0$ and $\psi = V$, for the BE and TE electrodes, respectively, while a boundary condition of $T = 300$ K was applied for the outermost surface of the electrodes, due to their larger area with respect to the CF. For the CF a uniform initial density of $n_D = 1 \times 10^{22} cm^{-3}$ was defined in conjunction with the following boundary conditions, $\frac{\partial}{\partial x} n_D(x=0, t) = 0$

and $n_D(x=L, t) = 0$, where L the length of the filament. Taken into consideration the atomic density of oxygen atoms in rutile TiO_{2-x} and HfO_{2-x} , the maximum doping density chosen ($1 \times 10^{22} cm^{-3}$) corresponds to a relative atomic concentration of 11.1%, or one oxygen vacancy in about 10 oxygen atoms, which could interpret the transition from insulating to metallic conduction. The CF size was set to a diameter of 4 nm, in line with direct evaluations using conducting atomic force microscopy [12].

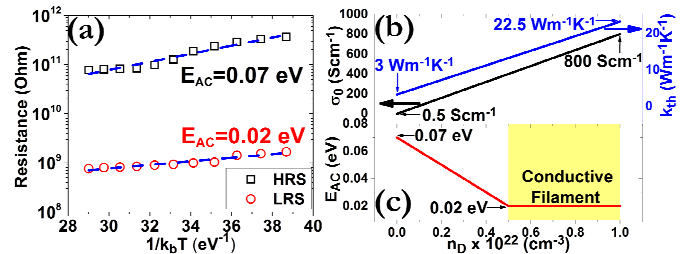


Fig. 1. (a) Measured activation energies for both HRS and LRS, (b) assumed electrical conductivity pre-exponential factor σ_0 , thermal conductivity k_{th} and (c) activation energy E_{AC} as a function of local doping density n_D .

Fig. 2(b) shows the measured and calculated I-V characteristics during SET/RESET transitions, respectively. The simulation profiles can capture the gradual character of the switching effect, while the physical picture can be viewed as the filling/depleting of a broken region within the CF and near the top electrode (TE), with V_o . The origins of the gradual responses can be found to the different dependence from the local electric field and temperature of the drift velocity and diffusivity (Fig. 3).

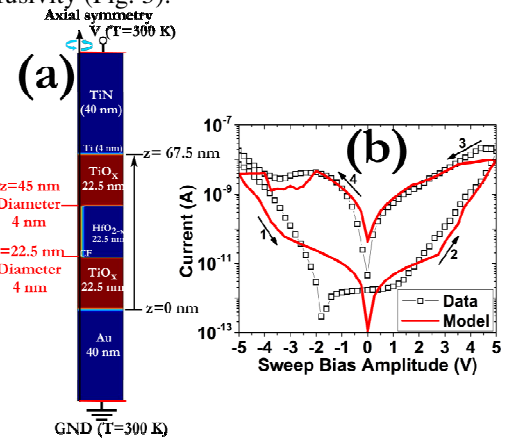


Fig. 2. (a) Simulated cell, (b) measured and calculated DC I-V characteristics.

The RESET transition begins at about -2 V and the current gradually decreases, achieving a difference of about one order of magnitude after $V_{\text{RESET}} = -5$ V. The physical origin for this effect is the creation of a small tunneling gap ($\sim 1-2$ nm – Fig. 4(a)) near the TE, which causes the decrease in the current values and enhanced locally the temperature and electric potential (Fig. 4(b), (c)). In contrast, during SET transition the continuum of the CF is restored (Fig. 4(d)) due to the generation of oxygen vacancies (Fig. 4(f)), causing the drop of the local temperature (Fig. 4(e)).

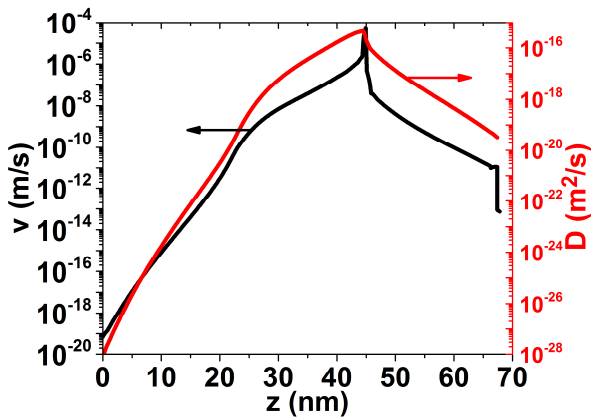


Fig. 3. Diffusivity and drift velocity as a function of vertical distance z.

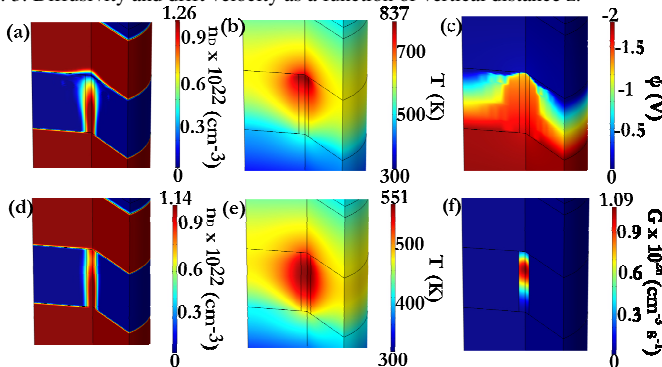


Fig. 4. Calculated maps of (a) V_o density, (b) temperature and (c) electric potential during RESET process (-2 V DC bias) and (d) V_o density, (e) temperature and (f) generation rate of V_o during SET process (5 V DC bias).

The model can also capture the analog properties of our devices, which should be regarded as promising result towards neuromorphic applications [13, 14]. In order to investigate whether the trilayer cells can be used as synaptic devices, we have measured the conductance change after the application of a train of 15 SET pulses, with amplitude 10 V and 10 ms width and repletion interval. As it can be seen from Fig. 5, the device potentiates (increases in conductance) after each pulse is applied, while depresses (decrease in conductance) when a train of 15 RESET pulses is applied on the same memory cell, with the same characteristics and negative amplitude. These results are similar to the short term synaptic plasticity effect which has been observed in biological synapses. The origins for these analog effects seem to be closely related with the processes of CF formation/annihilation. If we consider that

oxygen vacancies act as mediators for the electronic conduction, through trap/detrapping processes of electrons, the interplay between the two driving fluxes (drift and diffusion) dictates the switching pattern. Initially, during the SET process when the refilling of the gap begins, the high local electric field boosts the drift velocity, resulting in strong vertical V_o flux, as it is depicted in the calculated maps of n_D in Fig. 6 (states A-F). However, the small values of diffusivity result in negligible diffusion along the same direction with drift velocity, impeding the steep transition of the current (Fig. 7). The relatively high diffusion barrier of the dielectric stack is considered as the origin for these gradual transitions. Once the CF tip reaches the TE, the electric field and the local temperature are reduced and CF starts to increase in diameter, since now diffusion effect dominates. An even more gradual transition is observed for the RESET process, since the high temperatures affect both drift velocity and diffusivity (Fig. 8), but now the two fluxes have opposite direction (Fig. 6-states H-L). So, although the drift velocity is 10^3 times greater than in the SET transition, the gradual character of the switching effect is preserved. Consequently, it is apparent the interaction between the drift and diffusion effect can effectively tune the smooth switching pattern, which is clearly more apparent in pulse train mode.

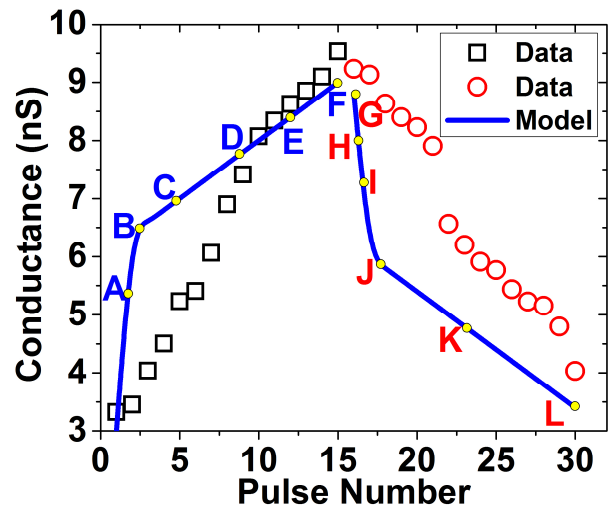


Fig. 5. Measured and calculated conductance changes under the application of a train of pulses ± 10 V pulses with 10 ms width.

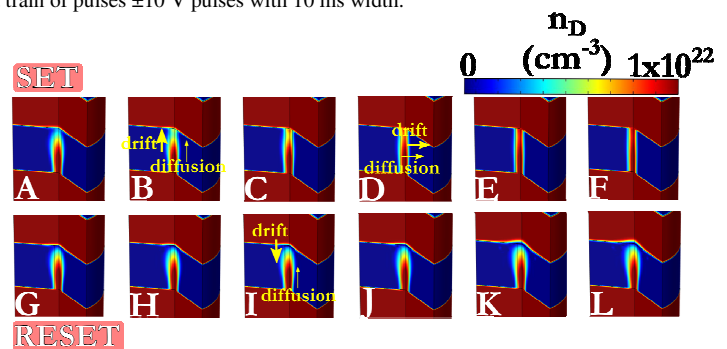


Fig. 6. Calculated 2D maps of n_D at different points during pulse training (states A-F correspond to SET pulses and states G-L to RESET pulses).

ACKNOWLEDGMENT

Two of the authors (P. Bousoulas and D. Tsoukalas) would like to acknowledge financial support from research program “Aristeia II” (Grant No. 4543). This research has been co-financed by the European Union (European Social Fund ESF) and Greek national funds through the Operational Program “Education and Lifelong Learning” of the National Strategic Reference Framework (NSRF).

REFERENCES

- [1] L. Chua, “Resistance Switching Memories Are Memristors”, *Appl. Phys. A: Mater. Sci. Process.*, vol. 102, p.p. 765–783, March 2011.
- [2] S. Yu, Y. Wu, R. Jeyasingh, D. Kuzum, H.-S. P. Wong, “An Electronic Synapse Device Based on Metal Oxide Resistive Switching Memory for Neuromorphic Computation”, *IEEE Trans. Electron Devices*, vol. 58, p.p. 2729–2737, Aug. 2011.
- [3] S. Ambrogio, S. Balatti, F. Nardi, S. Facchinetti, D. Ielmini, “Spike-Timing Dependent Plasticity in a Transistor- Selected Resistive Switching Memory”, *Nanotechnology*, vol. 24, p.p. 384012–384012, Sept. 2013.
- [4] J.-Y. Chen, C.-W. Huang, C.-H. Chiu, Y.-T. Huang, and W.-W. Wu, “Switching Kinetic of VCM-Based Memristor: Evolution and Positioning of Nanofilament”, *Adv. Mater.*, vol. 27, p.p. 5028–5033, July 2015.
- [5] K. Kamiya, M. Y. Yang, B. M.-Köpe, M. Niwa, Y. Nishi, and K. Shiraishi, “Vacancy Cohesion-Isolation Phase Transition Upon Charge Injection and Removal in Binary Oxide-Based RRAM Filamentary-Type Switching”, *IEEE Trans. on Elec. Dev.*, vol. 60, no.10, p.p. 3400–3406, Sept. 2013.
- [6] K. M. Kim, S. R. Lee, S. Kim, M. Chang, and C. S. Hwang, “Self-Limited Switching in Ta₂O₅/TaO_x Memristors Exhibiting Uniform Multilevel Changes in Resistance”, *Adv. Funct. Mater.*, vol. 25, p.p. 1527–1534, Jan. 2015.
- [7] Y. Yang, S. Choi, W. Lu, “Oxide Heterostructure Resistive Memory”, *Nano Lett.*, Vol. 13, p.p. 2908–2915, May 2013.
- [8] W. J. Ma, S. P. Lin, J. M. Luo, X. Y. Zhang, Ying Wang, Z. X. Li, B. Wang, and Yue Zheng, “Highly uniform bipolar resistive switching characteristics in TiO₂/BaTiO₃/TiO₂ multilayer”, *Appl. Phys. Lett.*, vol. 103, p.p. 262903-1 – 262903-5, Dec. 2013.
- [9] S. Larentis, F. Nardi, S. Balatti, D. C. Gilmer, and D. Ielmini, “Resistive Switching by Voltage-Driven Ion Migration in Bipolar RRAM—Part II: Modeling”, *IEEE Trans. on Elec. Dev.*, vol. 59, no. 9 p.p. 2468–2475, June 2012.
- [10] S. Kim, S.-J. Kim, K. M. Kim, S. R. Lee, M. Chang, E. Cho, Y.-B. Kim, C. J. Kim, U.-I. Chung & I.-K. Yoo, “Physical electro-thermal model of resistive switching in bi-layered resistance-change memory”, *Nat. Sci. Rep.*, vol. 3, p.p. 1680-1–1680-6, April 2013.
- [11] D. Ielmini, F. Nardi, and C. Cagli, “Physical models of size-dependent nanofilament formation and rupture in NiO resistive switching memories”, *Nanotechnology*, vol. 22, p.p. 254022-1 - 254022-12, May 2011.
- [12] M. Lanza, G. Bersuker, M. Porti, E. Miranda, M. Nafria, X. Aymerich, “Resistive switching in hafnium dioxide layers: local phenomenon at grain boundaries”, *Appl. Phys. Lett.*, vol. 101, p.p. 193502-1 – 193502-5, Nov. 2012.
- [13] S. Kim, S.-H. Choi, W. Lu, “Comprehensive Physical Model of Dynamic Resistive Switching in an Oxide Memristor”, *ACS Nano*, Vol. 8, No. 3, p.p. 2369–2376, Feb. 2014.
- [14] T. Chang, S. H. Jo, W. Lu, “Short -Term Memory to Long-Term Memory Transition in a Nanoscale Memristor”, *ACS Nano*, Vol. 5, No 9, p.p. 7669–7676, Aug. 2011.

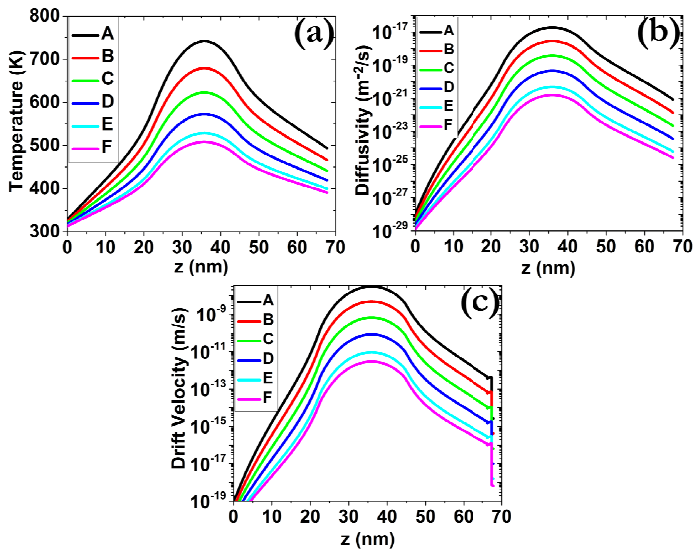


Fig. 7. Calculated 1D line profiles of T and drift velocity (v) and diffusivity (D) for states A-F.

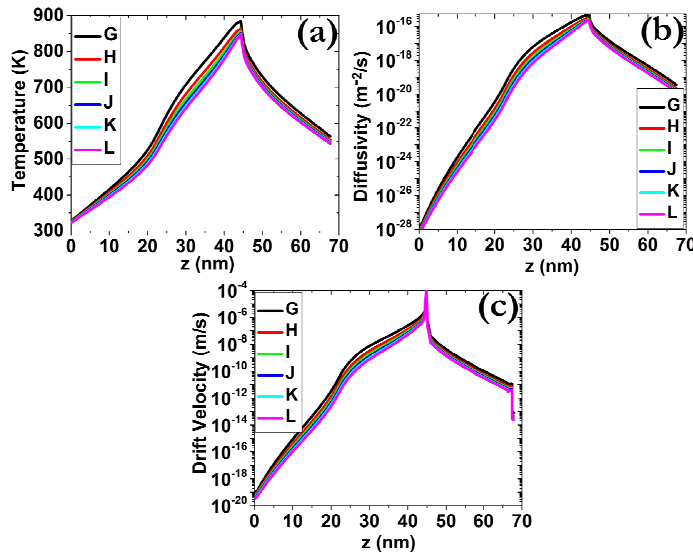


Fig. 8. Fig. 7. Calculated 1D line profiles of T and drift velocity (v) and diffusivity (D) for states G-L.

IV. CONCLUSIONS

In summary, a quantitatively approach was presented in order to interpret the switching effect in trilayer RRAM, by calculating self-consistently the distributions of local electric field, temperature and oxygen vacancy concentration. The model indicates that CF is formed/destroyed within the switching layer and closer to the TE, dominated by field and thermal effects. The strong competition between drift velocity and diffusivity, dictates the analog switching pattern, which was recorded in our devices and can be effectively tuned by choosing materials with differences in physical properties (i.e. diffusion barrier, hopping distance).